Precise temporal localisation of M/EEG effects with Bayesian generalised additive multilevel models

Ladislas Nalborczyk[1] and Paul Bürkner[2]
[1]Aix Marseille Univ, CNRS, LPL
[2]TU Dortmund University, Department of Statistics

Abstract

Time-resolved electrophysiological measurements such as those obtained through magneto- and electroencephalography (M/EEG) offer a unique window onto the neural activity underlying cognitive processes. Researchers are often interested in determining whether and when these signals differ across experimental conditions or participant groups. The conventional approach involves mass-univariate statistical testing across time and space followed by corrections for multiple comparisons or some form of cluster-based inference. While effective for controlling error rates at the cluster-level, cluster-based inference comes with a significant limitation: by shifting the focus of inference from individual time points to clusters, it prevents drawing conclusions about the precise onset or offset of observed effects. Here, we present a *model-based* alternative for analysing M/EEG timeseries, such as event-related potentials or time-resolved decoding accuracy. Our approach leverages Bayesian generalised additive multilevel models, providing posterior odds that an effect exceeds zero (or chance) at each time point, while naturally accounting for temporal dependencies and between-subject variability. Using both simulated and empirical M/EEG datasets, we show that this approach substantially outperforms conventional methods in estimating the onset and offset of neural effects, yielding more precise and reliable estimates. We provide an open-source R package implementing the method and describe how it can be integrated into M/EEG analysis pipelines using MNE-Python.

Keywords: EEG, MEG, cluster-based inference, multiple comparisons, generalised additive models, mixed-effects models, multilevel models, Bayesian statistics, brms

1 Introduction

1.1 Problem statement

Understanding the temporal dynamics of cognitive processes requires methods that can capture fast-changing neural activity with high temporal resolution. Magnetoencephalography and electroencephalography (M/EEG) are two such methods, widely used in cognitive neuroscience for their ability to track brain activity at the millisecond scale. These techniques provide rich time series data that reflect how neural responses unfold in response to stimuli or tasks. A central goal in many M/EEG studies is to determine whether, when, and where neural responses differ across experimental conditions or groups.

The conventional approach involves mass-univariate statistical testing through time and/or space followed by some form of correction for multiple comparisons with the goal of maintaining the familywise error rate (FWER) or the false discovery rate (FDR) at the nominal level (e.g., 5%). Cluster-based inference is the most common way of achieving this sort of error control in the M/EEG literature, being the recommended approach in several software programs (e.g., `EEGlab`, Delorme & Makeig, 2004; `MNE-Python`, Gramfort, 2013). While effective for controlling error rates, cluster-based inference comes with a significant limitation: by shifting the focus of inference from individual datapoints (e.g., timesteps, sensors, voxels) to clusters, it prevents the ability to draw precise conclusions about the spatiotemporal localisation of such effects (Maris & Oostenveld, 2007; Sassenhagen & Draschkow, 2019). As pointed out by Maris & Oostenveld (2007): "there is a conflict between this interest in localized effects and our choice for a global null hypothesis: by controlling the FA [false alarm] rate under this global null hypothesis, one cannot quantify the uncertainty in the spatiotemporal localization of the effect". Even worse, Rosenblatt et al. (2018) note that cluster-based inference suffers from low spatial resolution: "Since discovering a cluster means that 'there exists at least one voxel with an evoked response in the cluster', and not that 'all the voxels in the cluster have an evoked response', it follows that the larger the detected cluster, the less information we have on the location of the activation." As a consequence, cluster-based inference is expected to perform poorly for identifying the onset of M/EEG effects; a property that was later demonstrated in simulation studies (e.g., Rousselet, 2025; Sassenhagen & Draschkow, 2019).

To overcome the limitations of cluster-based inference, we introduce a novel *model-based* approach for precisely localising M/EEG effects in time, space, and other dimensions. The proposed approach, based on Bayesian generalised additive multilevel models, allows quantifying the posterior odds of effects being above chance at the level of timesteps, sensors, voxels, etc, while naturally taking into account spatiotemporal dependencies present in M/EEG data. We

Ladislas Nalborczyk https://orcid.org/0000-0002-7419-9855
Paul Bürkner https://orcid.org/0000-0001-5765-8995
The authors have no conflicts of interest to disclose.
Correspondence concerning this article should be addressed to Ladislas Nalborczyk, Aix Marseille Univ, CNRS, LPL, 5 avenue Pasteur, 13100 Aix-en-Provence, France, email: ladislas.nalborczyk@cnrs.fr

compare the performance of the proposed approach to well-established alternative methods using both simulated and actual M/EEG data and show that it significantly outperforms alternative methods in estimating the onset and offset of M/EEG effects.

1.2 Statistical errors and cluster-based inference

The issues with multiple comparisons represent a common and well-recognised danger in neuroimaging and M/EEG research, where the collected data allows for a multitude of potential hypothesis tests and is characterised by complex structures of spatiotemporal dependencies. The probability of obtaining at least one false positive in an ensemble (family) of m independent tests (i.e., the FWER) is computed as $1-(1-\alpha)^m$ (for $m = 10$ independent tests and $\alpha = 0.05$, it is approximately equal to 0.4). Different methods exist to control the FWER, that is, to bring it back to α. Most methods apply a simple correction to series of p-values issued from univariate statistical tests (e.g., t-tests). For instance, the Bonferroni correction (Dunn, 1961) consists in setting the significance threshold to α/m, or equivalently, multiplying the p-values by m and using the standard α significance threshold. This method is generally overconservative (i.e., under-powered) as it assumes statistical independence of the tests, an assumption that is clearly violated in the context of M/EEG timeseries characterised by massive spatiotemporal dependencies. Some alternative methods aims at controlling the FDR, defined as the proportion of false positive *among positive tests* (e.g., Benjamini & Hochberg, 1995; Benjamini & Yekutieli, 2001). However, a major limitation of both types of corrections is that they do not take into account the spatial and temporal information contained in M/EEG data.

A popular technique to account for spatiotemporal dependencies while controlling the FWER is cluster-based inference (Bullmore et al., 1999; Maris & Oostenveld, 2007). A typical cluster-based inference consists of two successive steps (for more details on cluster-based inference, see for instance Frossard & Renaud, 2022; Maris, 2011; Maris & Oostenveld, 2007; Sassenhagen & Draschkow, 2019). First, clusters are defined as sets of contiguous timesteps, sensors, voxels, etc, whose activity, summarised by some test statistic (e.g., a t-value), exceeds a predefined threshold (e.g., the 95th percentile of the parametric null distribution). Clusters are then characterised by their height (i.e., maximal value), extent (number of constituent elements), or some combination of both, for instance by summing the statistics within a cluster, an approach referred to as "cluster mass" (Maris & Oostenveld, 2007; Pernet et al., 2015). Then, the null hypothesis is tested by computing a p-value for each identified cluster by comparing its mass with the null distribution of cluster masses (obtained via permutation). As alluded previously, a significant cluster is a cluster which contains *at least one* significant time-point. As such, it would be incorrect to conclude, for instance, that the timestep of a significant cluster is the first moment at which some conditions differ (Frossard & Renaud, 2022; Sassenhagen & Draschkow, 2019). Because the inference is performed at the second step (i.e., once clusters have been formed), no conclusion can be made about individual datapoints (e.g., timesteps, sensors, etc).

As different cluster-forming thresholds lead to clusters with different spatial or temporal extent, this initial threshold modulates the sensitivity of the subsequent permutation test. The threshold-free cluster enhancement (TFCE) method was introduced by S. Smith & Nichols

(2009) to overcome this choice of an arbitrary threshold. In brief, the TFCE method works as follows. Instead of picking an arbitrary cluster-forming threshold (e.g., $t = 2$), the methods consist in trying all (or many) possible thresholds in a given range and checking whether a given datapoint (e.g., timestep, sensor, voxel) belongs to a significant cluster under any of the set of thresholds. Then, instead of using cluster mass, one uses a weighted average between the cluster extend (e, how broad is the cluster, that is, how many connected samples it contains) and the cluster height (h, how high is the cluster, that is, how large is the test statistic). The TFCE score at each timestep t is given by:

$$\text{TFCE(t)} = \int_{h=h_0}^{h=h_t} e(h)^E h^H \mathrm{d}h$$

where h_0 is typically 0 and parameters E and H are set a priori (typically to 0.5 and 2, respectively) and control the influence of the extend and height on the TFCE. In practice, this integral is approximated by a sum over small h increments. Then, a p-value for each timestep t is computed by comparing its TFCE with the null distribution of TFCE values (obtained via permutation). For each permuted signal, we keep the maximal value over the whole signal for the null distribution of the TFCE. The TFCE combined with permutation (assuming a large enough number of permutations) has been shown to provide accurate FWER control (e.g., Pernet et al., 2015). However, further simulation work showed that cluster-based methods (including TFCE) perform poorly in localising the onset of M/EEG effects (e.g., Rousselet, 2025; Sassenhagen & Draschkow, 2019).

To sum up, the main limitation of cluster-based inference is that it allows for inference at the cluster level only, not allowing inference at the level of timesteps, sensors, etc. As a consequence, it does not allow inferring the precise spatial and temporal localisation of effects. In the following, we briefly review previous modelling work of M/EEG data. Then, we provide a short introduction to generalised additive models (GAMs) to illustrate how these models can be used to precisely estimate the onset and offset of M/EEG effects.

1.3 Previous work on modelling M/EEG data

Scalp-recorded M/EEG signals capture neural activity originating from various brain regions and are often contaminated by artifacts unrelated to the cognitive processes under investigation. Consequently, analysing M/EEG data necessitates methods that can disentangle task-relevant neural signals from extraneous "noise." A widely adopted technique for this purpose is the estimation of event-related potentials (ERPs), which are stereotyped electrophysiological responses time-locked to specific sensory, cognitive, or motor events. Typically, ERPs are derived by averaging EEG or MEG epochs across multiple trials aligned to the event of interest (e.g., stimulus onset), thereby enhancing the signal-to-noise ratio by attenuating non-time-locked activity. However, this averaging approach has notable limitations: it assumes consistent latency and amplitude across trials and is primarily suited for simple categorical designs. Such assumptions may not hold in more complex experimental paradigms, potentially leading to suboptimal ERP estimations (e.g., N. J. Smith & Kutas, 2014a).

To overcome the limitations of simple averaging, several model-based approaches for estimating ERPs have been proposed. These methods are motivated by the observation that traditional ERP averaging is mathematically equivalent to fitting an intercept-only linear regression model in a simple categorical design without overlapping events (N. J. Smith & Kutas, 2014a). In contrast to simple averaging, regression-based approaches to ERP estimation offer substantially greater flexibility. Notably, they allow for the modelling of both linear and nonlinear effects of continuous predictors, such as word frequency or age (e.g., N. J. Smith & Kutas, 2014a, 2014b; Tremblay & Newman, 2014), and enable the disentangling of overlapping cognitive processes (e.g., Ehinger & Dimigen, 2019; Skukies et al., 2024; Skukies & Ehinger, 2021). One widely used implementation of this approach is provided by the LIMO EEG toolbox (Pernet et al., 2011), which follows a multi-stage analysis pipeline. First, a separate regression model is fit for each datapoint (e.g., each time point and electrode) at the individual participant level to estimate ERP responses. This is followed by group-level statistical analyses of the resulting regression coefficients, often accompanied by corrections for multiple comparisons or cluster-based inference (for recent applied examples, see Dunagan et al., 2025; Wüllhorst et al., 2025).

Although this framework allows for the inclusion of a wide range of predictors–both continuous and categorical, linear and nonlinear–it still has important limitations. First, fitting separate models for each datapoint ignores the spatiotemporal dependencies inherent in M/EEG data, potentially reducing statistical power and interpretability. Second, the subsequent group-level analyses typically do not account for hierarchical dependencies which could otherwise be addressed through multilevel modelling. Finally, because the output of this procedure is summarised by cluster-based inference, its conclusions remain subject to the limitations discussed in the previous section.

Beyond modelling nonlinear effects of continuous predictors on ERP amplitudes, GAMs have been employed to capture the temporal dynamics of ERPs themselves, effectively modelling the shape of the waveform over time (Abugaber et al., 2023; Baayen et al., 2018; Meulman et al., 2015, 2023). This approach allows for the estimation of smooth, data-driven functions that characterise how neural responses evolve over time, offering a flexible alternative to traditional linear models. In the following section, we provide a brief introduction to GAMs, highlighting their applicability to M/EEG time series analysis and the advantages they offer over conventional methods.

1.4 Generalised additive models

In generalised additive models, the functional relationship between the predictors and the response variable is decomposed into a sum of low-dimensional non-parametric functions. A typical GAM has the following form:

$$y_i \sim \mathrm{EF}\left(\mu_i, \phi\right)$$

$$g\left(\mu_i\right) = \underbrace{\mathbf{A}_i\gamma}_{\text{parametric part}} + \underbrace{\sum_{j=1}^{J} f_j\left(x_{ij}\right)}_{\text{non-parametric part}}$$

where $y_i \sim \mathrm{EF}\left(\mu_i, \phi\right)$ denotes that the observations y_i are distributed as some member of the exponential family of distributions (e.g., Gaussian, Gamma, Beta, Poisson) with mean μ_i and scale parameter ϕ; $g(\cdot)$ is the link function, $\mathbf{A}_i$ is the ith row of a known parametric model matrix, γ is a vector of parameters for the parametric terms (to be estimated), f_j is a smooth function of covariate x_j (to be estimated as well). The smooth functions f_j are represented in the model as a weighted sum of K simpler, basis functions:

$$f_j\left(x_{ij}\right) = \sum_{k=1}^{K} \beta_{jk} b_{jk}\left(x_{ij}\right)$$

where β_{jk} is the weight (coefficient) associated with the kth basis function $b_{jk}()$ evaluated at the covariate value x_{ij} for the jth smooth function f_j. To clarify the terminology at this point: *splines* are functions composed of simpler functions. These simpler functions are called *basis functions* (e.g., cubic polynomial, thin-plate) and the set of basis functions is called a *basis*. Each basis function is weighted by its coefficient and the resultant spline is the sum of these weighted basis functions (Figure 1A). Splines coefficients are penalised (usually through the square of the smooth functions' second derivative) in a way that can be interpreted, in Bayesian terms, as a prior on the "wiggliness" of the function (Miller, 2025; Wood, 2017a). In other words, more complex (wiggly) basis functions are automatically penalised.

A detailed treatment of the technical underpinnings of GAMs is beyond the scope of this article (see reference books such as Hastie & Tibshirani, 2017; Wood, 2017a). However, it is worth emphasising that GAMs have been successfully applied to a wide range of time series data across the cognitive sciences, including pupillometry (e.g., Rij et al., 2019), articulography (e.g., Wieling, 2018), speech formant dynamics (e.g., Sóskuthy, 2021), neuroimaging data (e.g., Dinga et al., 2021), and event-related potentials (e.g., Abugaber et al., 2023; Baayen et al., 2018; Meulman et al., 2015, 2023). Their appeal for modelling M/EEG data lies in their ability to flexibly capture the complex shape of ERP waveforms without overfitting, through the use of smooth functions constrained by penalisation. Recent extensions, such as distributional GAMs (Rigby & Stasinopoulos, 2005; Umlauf et al., 2018), allow researchers to model not only the mean structure but also the variance (or scale) and other distributional properties as functions of predictors, a feature that has proven useful in modelling neuroimaging data (e.g., Dinga et al., 2021). Moreover, hierarchical or multilevel GAMs (E. J. Pedersen et al., 2019) provide a principled way to account for the nested structure of M/EEG data (e.g., trials within participants), enabling the inclusion of varying intercepts, slopes, and smoothers (as illustrated in Figure 1C-D). This approach mitigates the risk of overfitting and reduces the influence of outliers on smooth estimates (Baayen & Linke, 2020; Meulman et al., 2023).

Figure 1

Different types of GAMs. ***A****: GAMs predictions are computed as the weigthed sum (in black) of basis functions (here thin-plate basis functions, in grey).* ***B****: Constant-effect GAM, with 5 participants in colours and the group-level prediction in black.* ***C****: Varying-intercept + varying-slope GAMM (with constant smoother).* ***D****: Varying-intercept + varying-slope + varying-smoother GAMM. In this model, each participant gets its own intercept, slope, and degree of 'wiggliness' (smoother).*

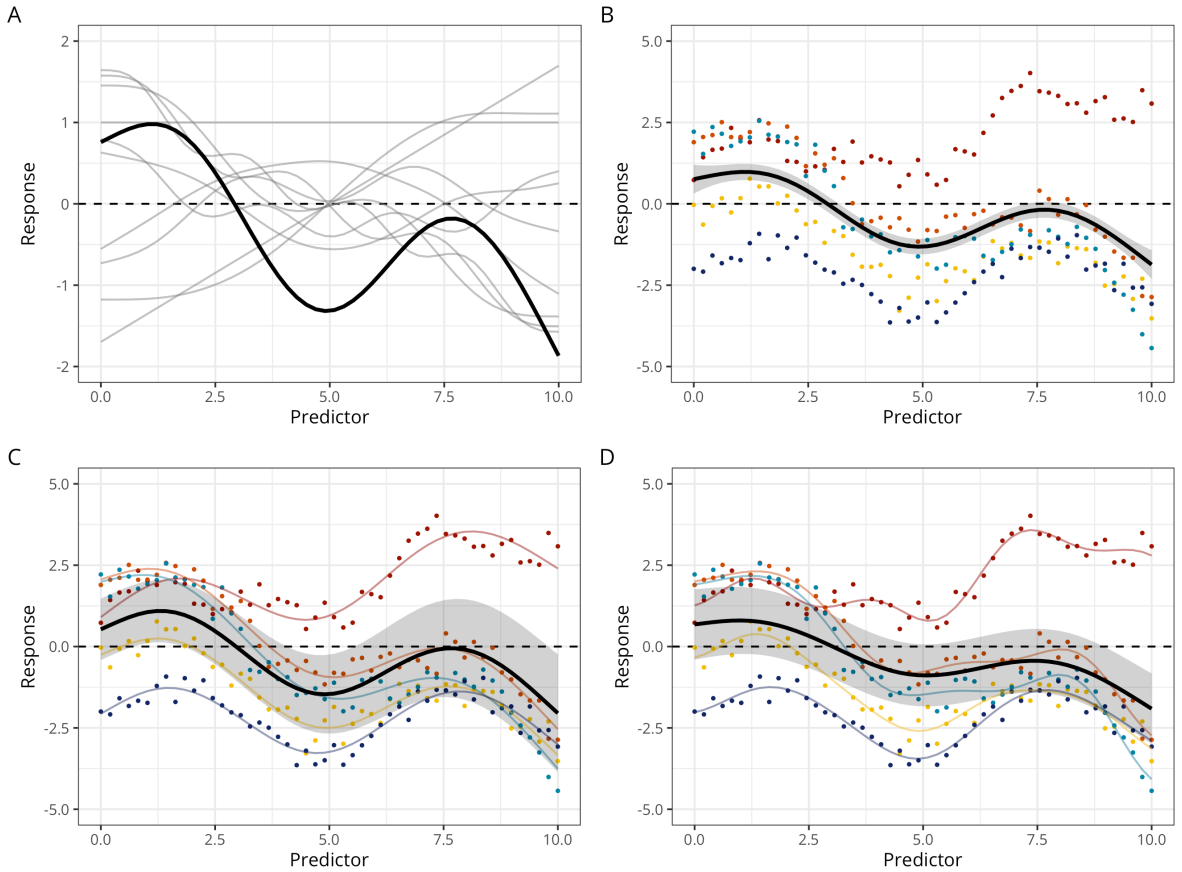

1.5 Objectives

Cluster-based permutation tests are widely used in M/EEG research to identify statistically significant effects across time and space. However, these methods have notable limitations, particularly in accurately determining the precise onset and offset of neural effects. To address these limitations, we developed a model-based approach relying on Bayesian generalised additive multilevel models implemented in `R` via the `brms` package (Bürkner, 2017, 2018). We evaluated the performance of this approach against conventional methods using both simulated and actual M/EEG data. Our findings demonstrate that this method provides more precise and reliable estimates of effects' onset and offset than conventional approaches such as cluster-based inference.

2 Benchmarking with known ground truth

2.1 Methods

2.1.1 M/EEG data simulation

To assess the accuracy of group-level onset and offset estimation of our proposed method, we simulated EEG with known onset and offset values. Following the approach of Sassenhagen & Draschkow (2019) and Rousselet (2025), we simulated EEG data stemming from two conditions, one with noise only, and the other with noise + signal. As in previous studies, the noise was generated by superimposing 50 sinusoids at different frequencies, following an EEG-like spectrum (see code in the online supplementary materials and details in Yeung et al., 2004). As in Rousselet (2025), the signal was generated from a truncated Gaussian distribution with an objective onset at 160 ms, a peak at 250 ms, and an offset at 342 ms. We simulated this signal for 250 timesteps between 0 and 0.5s, akin to a 500 Hz sampling rate. We simulated data for a group of 20 participants (with variable true onset) with 50 trials per participant and condition (Figure 2). All figures and simulation results can be reproduced using the `R` code available online at: https://github.com/lnalborczyk/brms_meeg.

Figure 2

Mean simulated EEG activity in two conditions with 50 trials each, for a group of 20 participants. The error band represents the mean +/- 1 standard error of the mean.

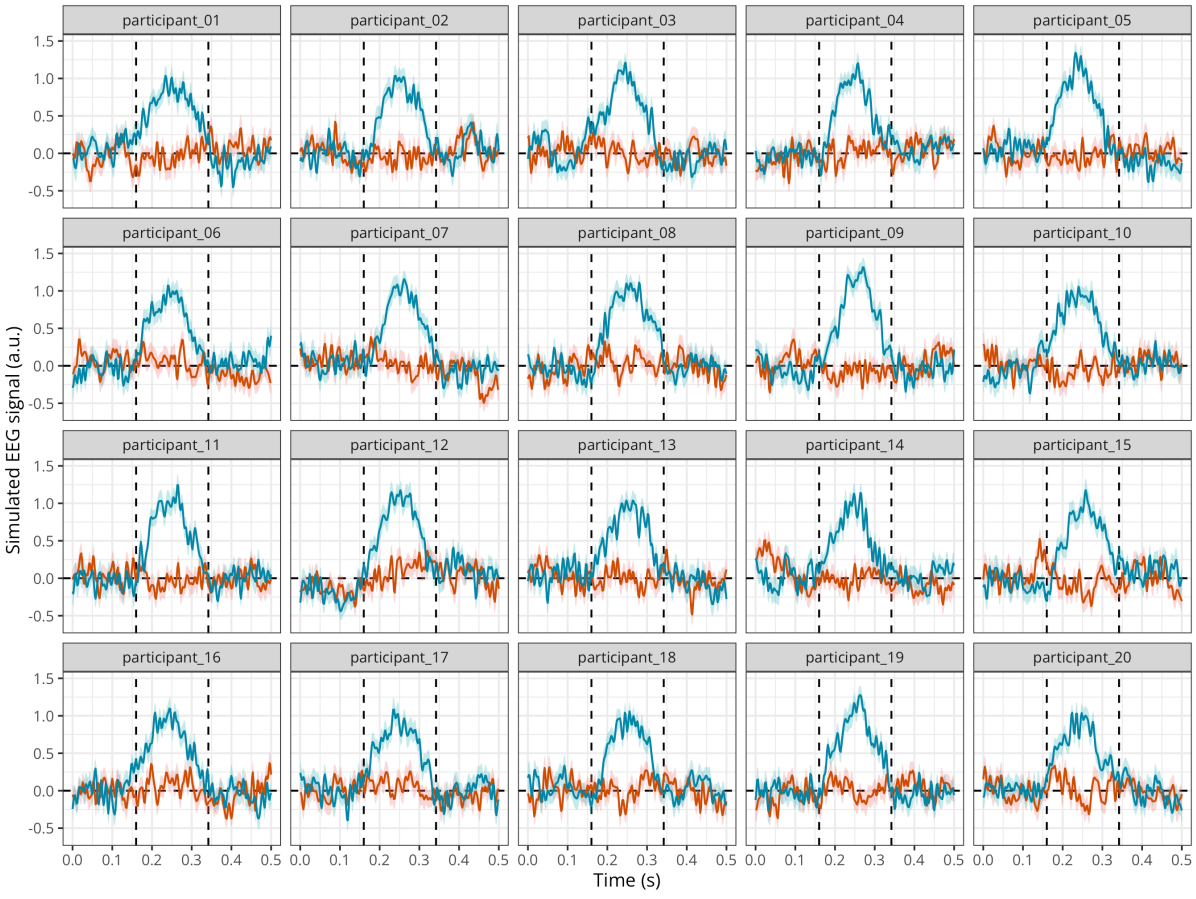

2.1.2 Model description and model fitting

We then fitted a Bayesian GAM (BGAM) using the `brms` package (Bürkner, 2017, 2018) and default priors (i.e., weakly informative priors). We ran eight Markov Chain Monte-Carlo (MCMC) to approximate the posterior distribution, including each 5000 iterations and a warmup of 2000 iterations, yielding a total of $8 \times (5000 - 2000) = 24000$ posterior samples to use for inference. Posterior convergence was assessed examining trace plots as well as the Gelman–Rubin statistic $\hat{R}$ (Gabry et al., 2019; Gelman et al., 2020; Vehtari et al., 2021). The `brms` package uses the same syntax as the `R` package `mgcv` v 1.9-3 (Wood, 2017b) for specifying smooth effects. Figure 3 shows the predictions of this model together with the raw data.

However, the model whose predictions are depicted in Figure 3 only included constant (fixed) effects, thus not properly accounting for between-participant variability. We next fitted a multilevel version of the BGAM (BGAMM, for an introduction to Bayesian multilevel models in `brms`, see Nalborczyk et al., 2019) including a varying intercept and slope for participant (but with a constant smoother). Although it is possible to fit a BGAMM using data at the single-trial level, we present a computationally lighter version of the model that is fitted directly on by-participant summary statistics (mean and SD), similar to what is done in meta-analysis.

We depict the posterior predictions together with the posterior estimate of the slope for `condition` at each timestep (Figure 3). This figure suggests that the BGAMM provides an adequate description of the simulated data (see further posterior predictive checks in Appendix B).

Figure 3

Posterior estimate of the EEG activity in each condition (left) and posterior estimate of the difference in EEG activity (right) according to the BGAMM.

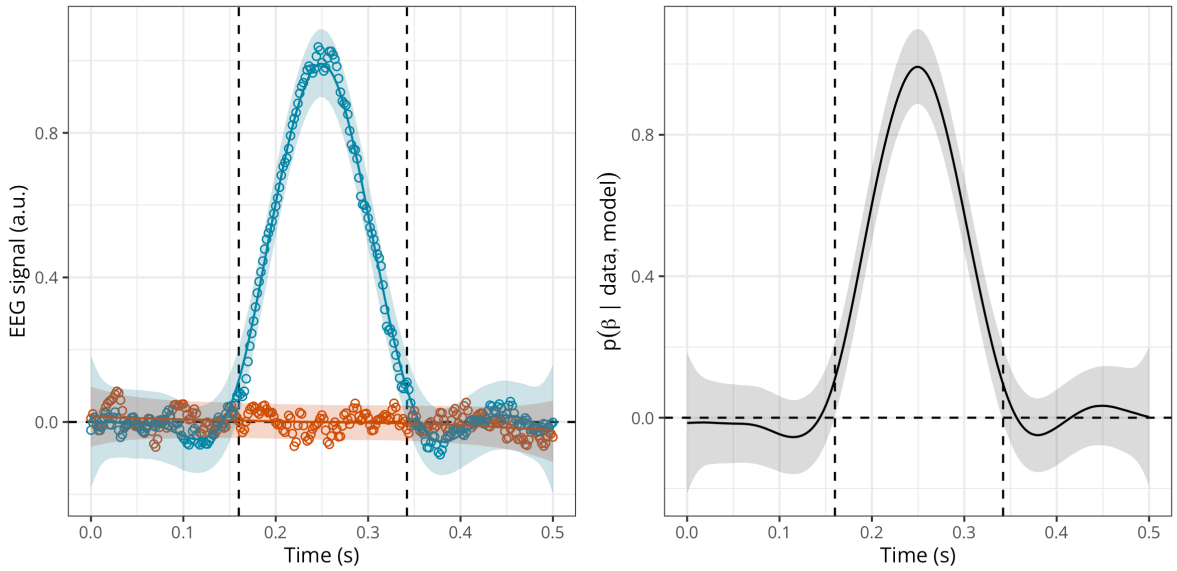

We then compute the posterior probability of the slope for `condition` being above 0 (Figure 4, left). From this quantity, we compute the ratio of posterior probabilities (i.e., $p/(1-p)$), or posterior odds, and visualise the timecourse of these odds superimposed with the conventional thresholds on evidence ratios (Figure 4, right). A ratio of 10 means that the probability of the

difference being above 0 is 10 times higher than the probability of the difference not being above 0, given the data, the priors, and other model's assumptions.[1] Thresholding the posterior odds thus provides a model-based approach for estimating the onset and offset of M/EEG effects, whose properties will be assessed in the simulation study. An important advantage is that the proposed approach can be extended to virtually any model structure.

Figure 4

Left: Posterior probability of the EEG difference (slope) being above 0 according to the BGAMM. Right: Posterior odds according to the BGAMM (on a log10 scale). Timesteps above threshold (10) are highlighted in green. NB: the minimum and maximum possible posterior odds are determined (bounded) by the number of posterior samples in the model.

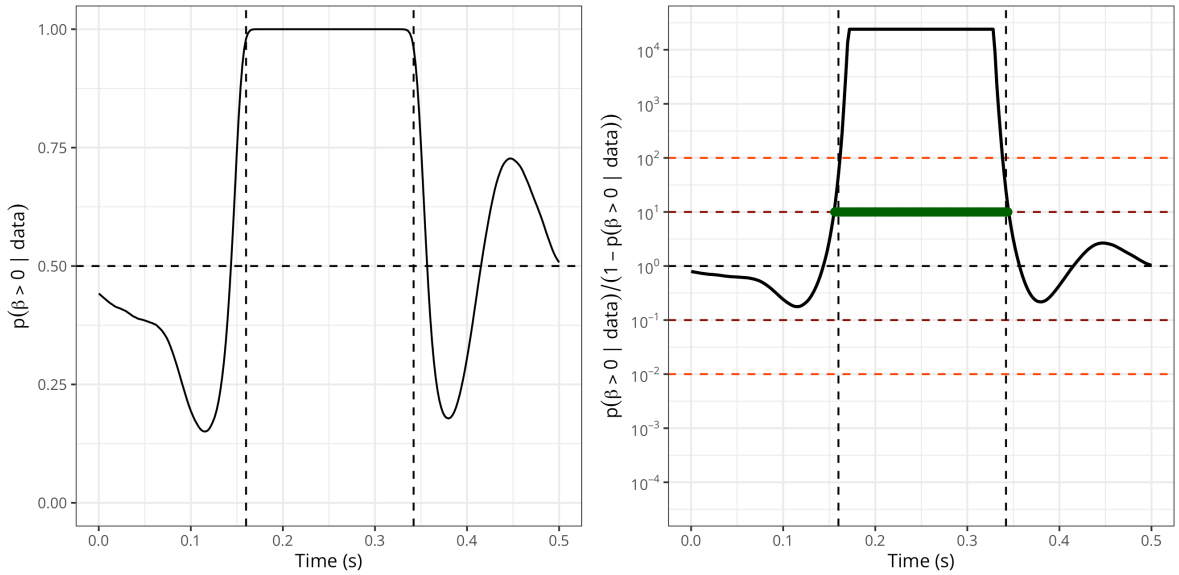

2.1.3 Comparing the onset/offset estimates across approaches

We then compared the ability of the BGAM to accurately estimate the onset and offset of the ERP difference to other widely-used methods. First, we conducted mass-univariate t-tests (thus treating each timestep independently) and identified the onset and offset of the ERP difference as the first and last values crossing an arbitrary significance threshold ($\alpha = 0.05$). We then followed the same approach but after applying different forms of multiplicity correction to the p-values. We compared two methods that control the FDR (i.e., `BH95`, Benjamini & Hochberg, 1995; and `BY01`, Benjamini & Yekutieli, 2001), one method that controls the FWER (i.e., Holm–Bonferroni method, Holm, 1979), and two cluster-based permutation methods (permutation with a single cluster-forming threshold and threshold-free cluster enhancement, `TFCE`, S. Smith & Nichols, 2009). The `BH95`, `BY01`, and `Holm` corrections were applied to the p-values using the `p.adjust()` function in `R`. The cluster-based inference was implemented using a cluster-sum statistic of squared t-values, as implemented in `MNE-Python` (Gramfort, 2013), called via the `R` package `reticulate` v 1.42.0 (Ushey et al., 2024). We also compared these estimates to the onset and offset as estimated using the binary segmentation algorithm, as implemented in the

[1] These posterior odds are equivalent to a Bayes factor, assuming 1:1 prior odds.

R package `changepoint` v 2.3 (Killick et al., 2022), and applied directly to the squared t-values (as in Rousselet, 2025).[2] Figure 5 illustrates the onsets and offsets estimated by each method on a single simulated dataset and shows that all methods systematically overestimate the true onset and underestimate the true offset. In addition, the `Raw p-value`, `FDR BH95`, and `FDR BY01` methods identify clusters well before the true onset and after the true offset.

Figure 5

Exemplary timecourse of squared t-values with true onset and offset (vertical black dashed lines) and onsets/offsets identified using the raw p-values, the corrected p-values (BH95, BY01, Holm), the cluster-based methods (Cluster mass, TFCE), or using the binary segmentation method (Change point).

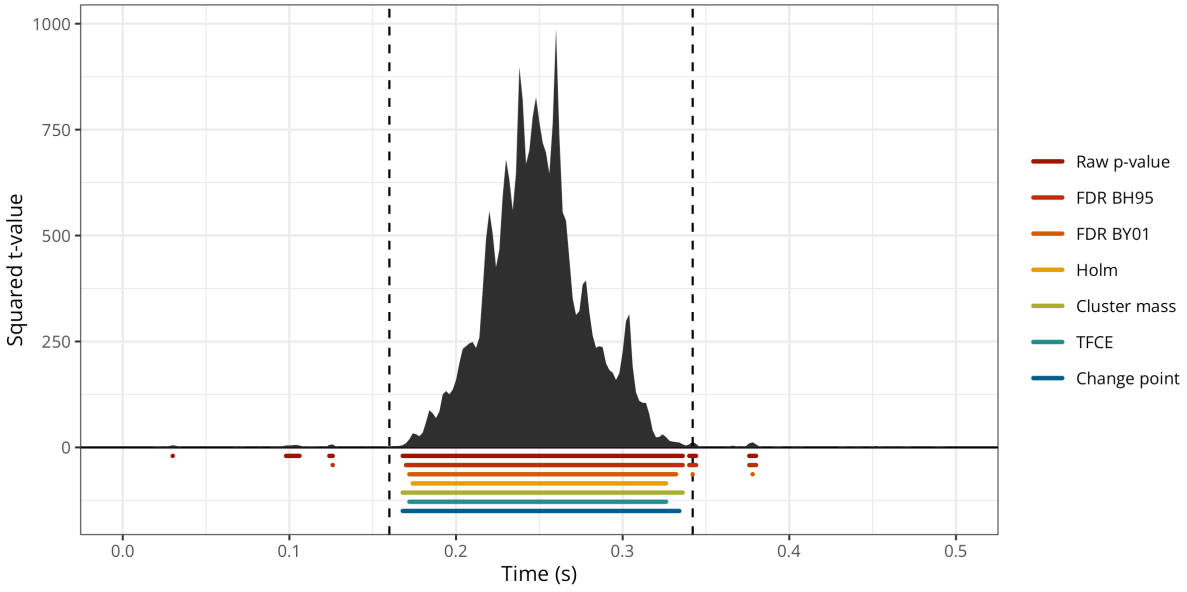

2.1.4 Simulation study

To assess the accuracy of group-level onset and offset estimation, all methods were compared by computing the bias (defined as the mean difference between the estimated and true value of the onset/offset), mean absolute error (MAE), root mean square error (RMSE), and variance of onset/offset estimates from 10,000 simulated datasets. Following Rousselet (2025), each participant was assigned a random onset between 150 and 170ms. Whereas the present article focuses on one-dimensional signals (e.g., one M/EEG channel), we provide a 2D application in Appendix A.

2.2 Results

Figure 6 shows a summary of the simulation results, revealing that the proposed approach (`BGAM`) has the lowest error for both the onset and offset estimates. The `Cluster mass` and `Change point` methods also have good performance, but perhaps surprisingly, the `TFCE` method performs

[2] As in Rousselet (2025), we fixed the number of expected change points to two in the binary segmentation algorithm, thus producing always one cluster.

poorly for estimating the offset of the effect (with performance similar to the `Holm` method). Unsurprisingly, the `FDR BH95` and `Raw p-value` methods show the worst performance.

Figure 6

Mean error and variance of onset and offset estimates according to each method. Variance is plotted on a log10 scale for visual purposes.

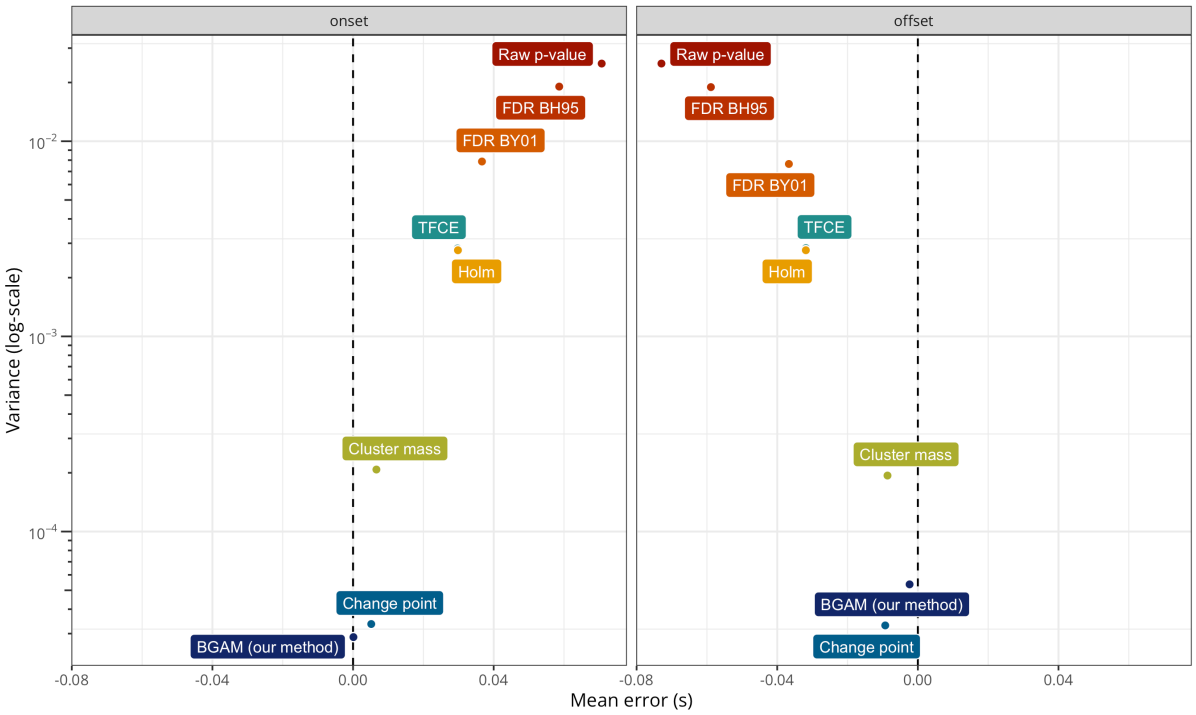

These results are further summarised in Table 1, which shows that the `BGAM` method is almost perfectly unbiased (i.e., it has a bias of approximately 0.1ms for the onset and 2.4ms for the offset). The `Bias` column shows that all methods tend to estimate the onset later than the true onset and to estimate the offset earlier than the true offset. As can be seen from this table, the `BGAM` method has the best performance on all included metrics (except for the `Variance` of the offset estimate, where the `Change point` method performs better, presumably because it was constrained to identifying a single cluster).

3 Application to actual MEG data

3.1 Methods

To complement the simulation study, we evaluated the performance of all methods on actual MEG data (Nalborczyk et al., in preparation). In this study, the authors conducted time-resolved multivariate pattern analysis (MVPA, also known as decoding) of MEG data recorded in 32 human participants during a reading task. As a result, the authors obtained a timecourse of decoding accuray (ROC AUC), bounded between 0 and 1, for each participant. To test whether the group-level average decoding accuracy was above chance (i.e., 0.5) at each timestep, we fitted a BGAM as introduced previously with a basis dimension $k = 50$ and retained all timesteps exceeding a posterior odds of 20. To better distinguish signal from noise, we defined a region of

Table 1

Summary statistics of onset/offset estimates for each method (in ms, ordered by the MAE).

	Bias	MAE	RMSE	Variance
onset				
BGAM (our method)	**0.11**	**2.76**	**0.11**	**28.78**
Change point	5.17	6.51	5.17	33.58
Cluster mass	6.64	7.62	6.64	207.86
Holm	29.83	32.01	29.83	2,763.68
TFCE	29.73	32.07	29.73	2,823.11
FDR BY01	36.67	50.80	36.67	7,872.30
FDR BH95	58.64	102.49	58.64	19,054.58
Raw p-value	70.72	132.86	70.72	25,004.65
offset				
BGAM (our method)	**-2.35**	**3.46**	**2.35**	53.63
Cluster mass	-8.64	9.44	8.64	193.63
Change point	-9.28	9.82	9.28	**33.03**
Holm	-31.86	34.03	31.86	2,764.12
TFCE	-31.84	34.19	31.84	2,834.11
FDR BY01	-36.68	51.37	36.68	7,648.53
FDR BH95	-58.87	102.63	58.87	18,939.58
Raw p-value	-72.93	133.33	72.93	25,012.72

practical equivalence (ROPE, Kruschke & Liddell, 2017) as the upper 90% quantile of decoding performance during the baseline period (i.e., before stimulus onset). Although we chose a basis dimension of $k = 50$, which seemed appropriate for the present data, this choice should be adapted according to the properties of the modelled data (e.g., signal-to-noise ratio, prior low-pass filtering, sampling rate) and should be assessed by the usual model checking tools (e.g., models comparison, posterior predictive checks, see Appendix B).

3.2 Results

Figure 7 shows the group-level average decoding performance through time superimposed with onset and offset estimates from each method. Overall, this figure shows that both the `Raw p-value` and `FDR BH95` methods are extremely lenient, identifying clusters of above-chance decoding accuracy before the onset of the stimulus (false positive) and until the end of the trial. The `Change point` method seems to be the most conservative one, identifying a single cluster spanning from approximately +60ms to +450ms. The `Holm`, `Cluster mass`, `TFCE`, and `BGAM` methods produce roughly similar estimates of onset and offset, ranging from approximately +60ms to +650ms (considering only the first and last identified timesteps), although the `BGAM` method seems to result in fewer clusters.

We then assessed the sensitivity of the various methods using a form of permutation-based sensitivity study, which consisted of the following steps. First, we created a large number of split halves of the data, that is, subsets of the dataset containing only 16 out of 32 participants. For each possible pair of subsets, we have 16 possible levels of overlap/similarity that can be quantified using the Jaccard index, ranging from 0 (perfectly disjoints subsets) to ≈ 0.88 (identical subsets except one participant). For each of these 16 levels of Jaccard similarity, we

Figure 7

Group-level average decoding performance through time with clusters of higher-than-chance decoding performance as identified by each method (data from Nalborczyk et al., in preparation).

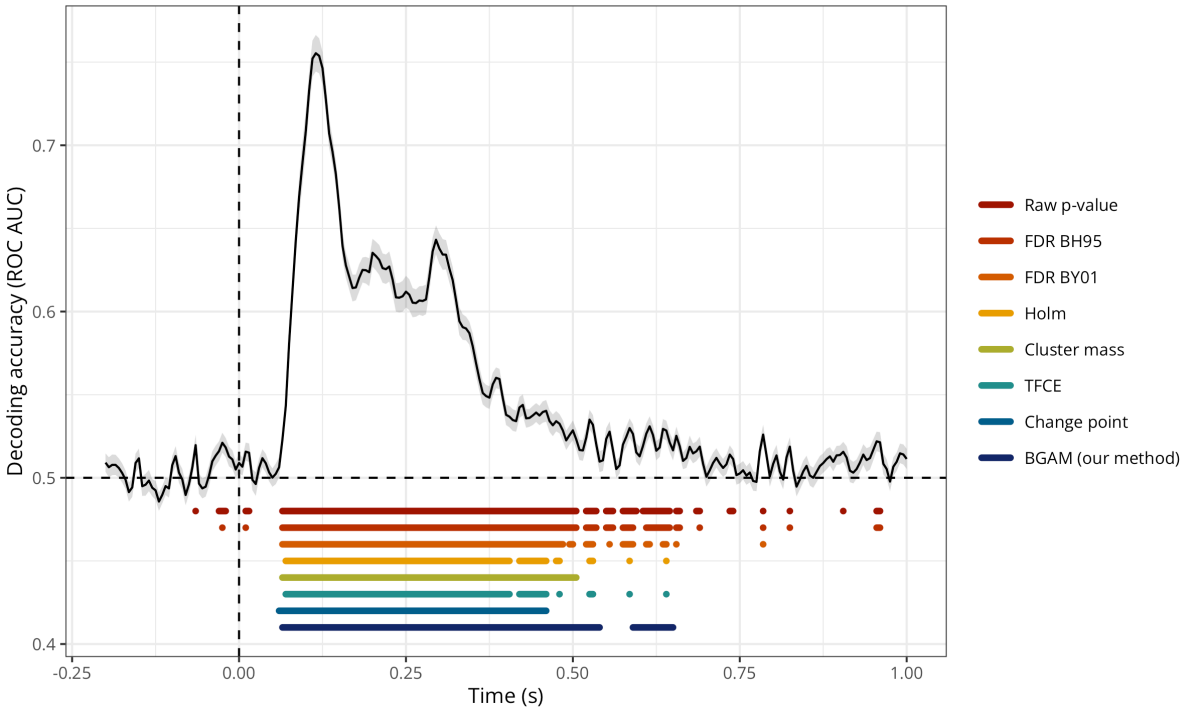

created 1,000 pairs of subsets, resulting in 16,000 pairs of subsets in total. For each of these pairs, we estimated the onset and offset according to each method and computed the absolute difference in onset/offset estimates. Finally, we estimated the Spearman's rank correlation coefficient (which quantifies the strength of a monotonic relation between two variables) between the Jaccard similarity and the absolute difference in onset/offset estimates. The rational for this procedure is that sensitive methods should produce similar onset/offset estimates for similar subsets and dissimilar onset/offset estimates for dissimilar subsets. The results of this procedure are summarised in Figure 8.

This figure shows that, among the methods that performed best in the simulation study (i.e., `Cluster mass`, `Change point`, and `BGAM`), onset estimates remain highly stable across subsets of participants with varying Jaccard similarity, it varies from around 1ms for most similar subsets to around 10ms for most dissimilar subsets. Additionally, for both onset and offset estimates, the average pairwise difference increases monotonically with Jaccard dissimilarity, as indicated by the Spearman's rank correlation coefficient. For the onset estimates, the `Holm`, `Cluster mass`, `TFCE`, and `BGAM` methods exhibit the strongest monotonic relation with subset similarity (all ρs > 0.9), whereas for offset estimates, all methods demonstrate excellent performance (all ρs > 0.9) with the `BGAM` method showing the highest sensitivity ($\rho \approx 0.994$). However, given the aberrant clusters identified by the `Raw p-value`, `FDR BH95`, and `FDR BY01` methods (see Figure 7), their sensitivity to variation in subset similarity is not meaningful.

Figure 8

Relation between data subsets' dissimilarity (x-axis) and difference in onset (blue) and offset (orange) estimates (y-axis) according to each method.

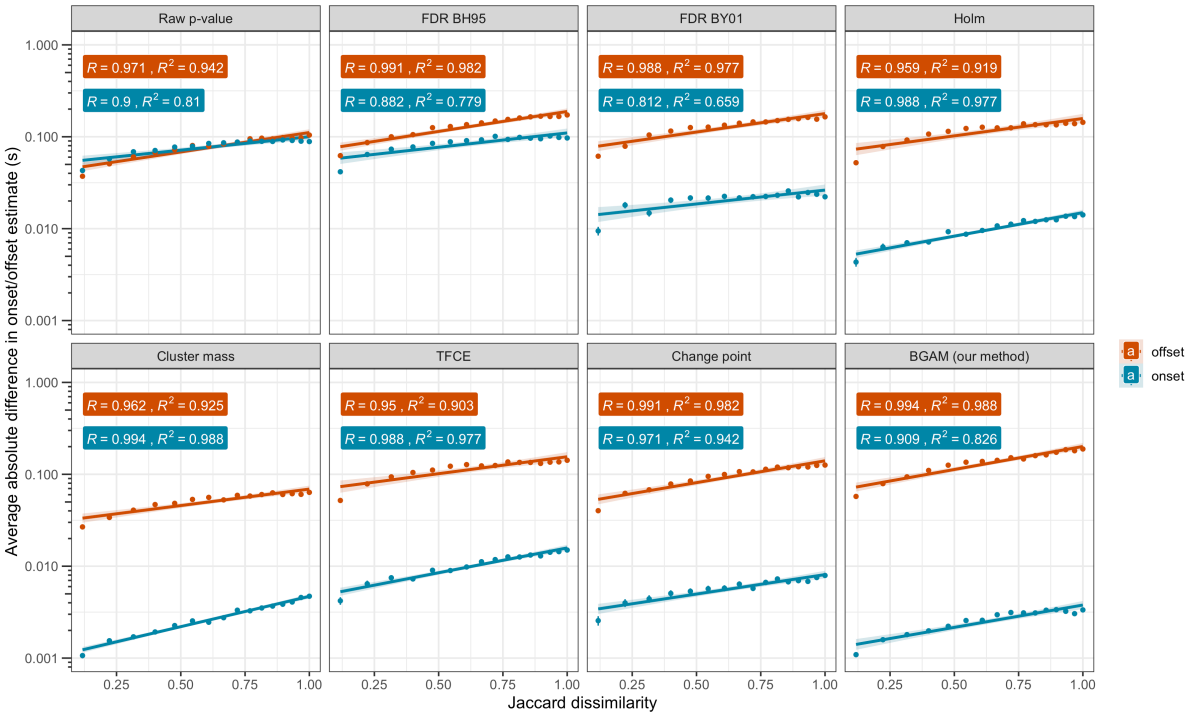

4 Discussion

In brief, our results show that the model-based approach we introduced outperforms conventional cluster-based methods in identifying the onset and offset of M/EEG effects. We first assessed the performance of this approach on simulated data allowing us to evaluate the method's ability to recover ground-truth onset and offset values. We then assessed its performance on actual MEG data, allowing us to assess its sensitivity to realistic data properties (subset similarity). Together, these results highlight desirable properties for any method aiming to precisely and reliably estimate the onset and offset of M/EEG effects: it should i) recover true onsets and offsets in simulation (good asymptotic behaviour), ii) identify clusters that are interpretable and consistent in empirical data, and iii) show sensitivity to subtle changes in the data. Our approach meets all three of these desiderata.

As with previous simulation studies (e.g., Rousselet et al., 2008; Sassenhagen & Draschkow, 2019), results inevitably depend on design choices, including the specific cluster-forming algorithm and threshold (for cluster-based methods), the signal-to-noise ratio, and the potential degradation of temporal resolution introduced by preprocessing steps such as low-pass filtering. However, these constraints apply equally to all methods tested, so relative differences in performance remain meaningful.

Interestingly, the TFCE method performed worse than the traditional cluster-sum approach, consistent with the predictions of Rousselet (2025) based on the original findings of S. Smith & Nichols (2009). We also found a striking overlap in the clusters identified by the `Holm` and

`TFCE` procedures (cf. Figure 7 and Figure 8). Whereas these two approaches are conceptually distinct; `Holm` controlling the family-wise error rate through sequential p-value adjustment, `TFCE` enhancing signal based on spatiotemporal support; their similarity in practice may arise because both effectively prioritise extended, moderately strong effects over isolated high-intensity points. This convergence warrants further methodological work.

A critical requirement for any model-based approach is that the model must adequately capture the underlying data-generating process. Misspecified models are likely to produce biased or unreliable onset/offset estimates. This underscores the importance of thorough model diagnostics, including posterior predictive checks, fit assessments, and model comparison (Gelman et al., 2020). An important and related methodological consideration concerns the selection of model hyperparameters, such as the number of basis functions and the threshold for posterior odds. Although our simulations suggest that these parameters influence the precision and reliability of onset and offset estimates, optimal values may vary depending on the signal's temporal dynamics and signal-to-noise characteristics. Future work could explore principled approaches to hyperparameter tuning, including cross-validation or fully Bayesian model selection using tools such as leave-one-out cross-validation (LOO-CV) or Bayes factors (Gelman et al., 2020). We provide initial guidance in Appendix B and advocate for future development of adaptive heuristics to support flexible yet parsimonious model specification.

Currently, our approach estimates temporal effects independently at each sensor (1D temporal data). Extending the current framework to incorporate additional temporal (see Appendix A) or spatial dimensions would improve both sensitivity and interpretability. Such extensions could draw on methods from spatial epidemiology and geostatistics using either GAMMs or approximate Gaussian process regression (e.g., Rasmussen & Williams, 2005; Riutort-Mayol et al., 2023), depending on computational feasibility.

To facilitate adoption, we developed the `neurogram` open-source `R` package (Nalborczyk, 2025), which implements the proposed method using `brms`. The package integrates seamlessly with `MNE-Python` (Gramfort, 2013), enabling researchers to process M/EEG data in `Python` and import them directly into `R` for model-based inference without cumbersome data export. This interoperability, described in Appendix C, is designed to encourage broader use of model-based approaches in cognitive neuroscience.

In conclusion, we introduced a model-based approach for estimating the onset and offset of M/EEG effects. Across simulated and empirical datasets, we showed that the method yields more precise and sensitive estimates than conventional cluster-based approaches. These results highlight the potential of flexible, model-based alternatives for characterising time-resolved neural dynamics, particularly in applications where accurate temporal localisation is critical.

Data and code availability

The simulation results as well as the `R` code to reproduce the simulations are available at: https://github.com/lnalborczyk/brms_meeg. The `neurogam R` package is available at https://github.com/lnalborczyk/neurogam.

Packages

We used R version 4.4.3 (R Core Team, 2025) and the following R packages: assertthat v. 0.2.1 (Wickham, 2019), brms v. 2.22.0 (Bürkner, 2017, 2018, 2021), doParallel v. 1.0.17 (Corporation & Weston, 2022), foreach v. 1.5.2 (Microsoft & Weston, 2022), furrr v. 0.3.1 (Vaughan & Dancho, 2022), future v. 1.58.0 (Bengtsson, 2021), ggpubr v. 0.6.0 (Kassambara, 2023), ggrepel v. 0.9.6 (Slowikowski, 2024), glue v. 1.8.0 (Hester & Bryan, 2024), grateful v. 0.2.12 (Rodriguez-Sanchez & Jackson, 2024), gt v. 1.0.0 (Iannone et al., 2025), knitr v. 1.50 (Xie, 2014, 2015, 2025), MetBrewer v. 0.2.0 (Mills, 2022), mgcv v. 1.9.3 (Wood, 2003b, 2004, 2011, 2017c; Wood et al., 2016), neurogam v. 0.0.1 (Nalborczyk, 2025), pakret v. 0.2.2 (Gallou, 2024), patchwork v. 1.3.0 (T. L. Pedersen, 2024), rmarkdown v. 2.29 (Allaire et al., 2024; Xie et al., 2018, 2020), scales v. 1.4.0 (Wickham et al., 2025), scico v. 1.5.0 (T. L. Pedersen & Crameri, 2023), signal v. 1.8.1 (signal developers, 2023), tictoc v. 1.2.1 (Izrailev, 2024), tidybayes v. 3.0.7 (Kay, 2024), tidytext v. 0.4.2 (Silge & Robinson, 2016), tidyverse v. 2.0.0 (Wickham et al., 2019).

Acknolwedgements

Centre de Calcul Intensif d'Aix-Marseille is acknowledged for granting access to its high performance computing resources.

References

Abugaber, D., Finestrat, I., Luque, A., & Morgan-Short, K. (2023). Generalized additive mixed modeling of EEG supports dual-route accounts of morphosyntax in suggesting no word frequency effects on processing of regular grammatical forms. *Journal of Neurolinguistics*, *67*, 101137. https://doi.org/10.1016/j.jneuroling.2023.101137

Allaire, J., Xie, Y., Dervieux, C., McPherson, J., Luraschi, J., Ushey, K., Atkins, A., Wickham, H., Cheng, J., Chang, W., & Iannone, R. (2024). *rmarkdown: Dynamic documents for r*. https://github.com/rstudio/rmarkdown

Baayen, R. H., & Linke, M. (2020). *Generalized Additive Mixed Models* (pp. 563–591). Springer International Publishing. https://doi.org/10.1007/978-3-030-46216-1_23

Baayen, R. H., Rij, J. van, Cat, C. de, & Wood, S. (2018). *Autocorrelated errors in experimental data in the language sciences: Some solutions offered by generalized additive mixed models* (pp. 49–69). Springer International Publishing. https://doi.org/10.1007/978-3-319-69830-4_4

Bengtsson, H. (2021). A unifying framework for parallel and distributed processing in r using futures. *The R Journal*, *13*(2), 208–227. https://doi.org/10.32614/RJ-2021-048

Benjamini, Y., & Hochberg, Y. (1995). Controlling the False Discovery Rate: A Practical and Powerful Approach to Multiple Testing. *Journal of the Royal Statistical Society Series B: Statistical Methodology*, *57*(1), 289–300. https://doi.org/10.1111/j.2517-6161.1995.tb02031.x

Benjamini, Y., & Yekutieli, D. (2001). The control of the false discovery rate in multiple testing under dependency. *The Annals of Statistics*, *29*(4). https://doi.org/10.1214/aos/1013699998

Bullmore, E. T., Suckling, J., Overmeyer, S., Rabe-Hesketh, S., Taylor, E., & Brammer, M. J. (1999). Global, voxel, and cluster tests, by theory and permutation, for a difference between two groups of structural MR images of the brain. *IEEE Transactions on Medical Imaging*, *18*(1), 32–42. https://doi.org/10.1109/42.750253

Bürkner, P.-C. (2017). brms: An R package for Bayesian multilevel models using Stan. *Journal of Statistical Software*, *80*(1), 1–28. https://doi.org/10.18637/jss.v080.i01

Bürkner, P.-C. (2018). Advanced Bayesian multilevel modeling with the R package brms. *The R Journal*, *10*(1), 395–411. https://doi.org/10.32614/RJ-2018-017

Bürkner, P.-C. (2021). Bayesian item response modeling in R with brms and Stan. *Journal of Statistical Software*, *100*(5), 1–54. https://doi.org/10.18637/jss.v100.i05

Corporation, M., & Weston, S. (2022). *doParallel: Foreach parallel adaptor for the "parallel" package*. https://CRAN.R-project.org/package=doParallel

Delorme, A., & Makeig, S. (2004). EEGLAB: an open source toolbox for analysis of single-trial EEG dynamics including independent component analysis. *Journal of Neuroscience Methods*, *134*(1), 9–21. https://doi.org/10.1016/j.jneumeth.2003.10.009

Dinga, R., Fraza, C. J., Bayer, J. M. M., Kia, S. M., Beckmann, C. F., & Marquand, A. F. (2021). *Normative modeling of neuroimaging data using generalized additive models of location scale and shape*. http://dx.doi.org/10.1101/2021.06.14.448106

Dunagan, D., Jordan, T., Hale, J. T., Pylkkänen, L., & Chacón, D. A. (2025). Evaluating the

timecourses of morpho-orthographic, lexical, and grammatical processing following rapid parallel visual presentation: An EEG investigation in English. *Cognition*, *257*, 106080. https://doi.org/10.1016/j.cognition.2025.106080

Dunn, O. J. (1961). Multiple Comparisons among Means. *Journal of the American Statistical Association*, *56*(293), 52–64. https://doi.org/10.1080/01621459.1961.10482090

Ehinger, B. V., & Dimigen, O. (2019). Unfold: An integrated toolbox for overlap correction, non-linear modeling, and regression-based EEG analysis. *PeerJ*, *7*, e7838. https://doi.org/10.7717/peerj.7838

Frossard, J., & Renaud, O. (2022). The cluster depth tests: Toward point-wise strong control of the family-wise error rate in massively univariate tests with application to M/EEG. *NeuroImage*, *247*, 118824. https://doi.org/10.1016/j.neuroimage.2021.118824

Gabry, J., Simpson, D., Vehtari, A., Betancourt, M., & Gelman, A. (2019). Visualization in Bayesian workflow. *Journal of the Royal Statistical Society: Series A (Statistics in Society)*, *182*(2), 389–402. https://doi.org/10.1111/rssa.12378

Gallou, A. (2024). *pakret: Cite "R" packages on the fly in "R Markdown" and "Quarto"*. https://CRAN.R-project.org/package=pakret

Gelman, A., Vehtari, A., Simpson, D., Margossian, C. C., Carpenter, B., Yao, Y., Kennedy, L., Gabry, J., Bürkner, P.-C., & Modrák, M. (2020). Bayesian workflow. *arXiv:2011.01808 [Stat]*. http://arxiv.org/abs/2011.01808

Gramfort, A. (2013). MEG and EEG data analysis with MNE-python. *Frontiers in Neuroscience*, *7*. https://doi.org/10.3389/fnins.2013.00267

Hastie, T. J., & Tibshirani, R. J. (2017). *Generalized Additive Models*. Routledge. https://doi.org/10.1201/9780203753781

Hester, J., & Bryan, J. (2024). *glue: Interpreted string literals*. https://CRAN.R-project.org/package=glue

Holm, S. (1979). A simple sequentially rejective multiple test procedure. *Scandinavian Journal of Statistics*, *6*(2), 65–70. http://www.jstor.org/stable/4615733

Iannone, R., Cheng, J., Schloerke, B., Hughes, E., Lauer, A., Seo, J., Brevoort, K., & Roy, O. (2025). *gt: Easily create presentation-ready display tables*. https://CRAN.R-project.org/package=gt

Izrailev, S. (2024). *tictoc: Functions for timing r scripts, as well as implementations of "Stack" and "StackList" structures*. https://CRAN.R-project.org/package=tictoc

Kassambara, A. (2023). *ggpubr: "ggplot2" based publication ready plots*. https://CRAN.R-project.org/package=ggpubr

Kay, M. (2024). *tidybayes: Tidy data and geoms for Bayesian models*. https://doi.org/10.5281/zenodo.1308151

Killick, R., Haynes, K., & Eckley, I. A. (2022). *changepoint: An R package for changepoint analysis*. https://CRAN.R-project.org/package=changepoint

King, J.-R., & Dehaene, S. (2014). Characterizing the dynamics of mental representations: the temporal generalization method. *Trends in Cognitive Sciences*, *18*(4), 203–210. https://doi.org/10.1016/j.tics.2014.01.002

Kruschke, J. K., & Liddell, T. M. (2017). The Bayesian New Statistics: Hypothesis testing,

estimation, meta-analysis, and power analysis from a Bayesian perspective. *Psychonomic Bulletin & Review*, *25*(1), 178–206. https://doi.org/10.3758/s13423-016-1221-4

Maris, E. (2011). Statistical testing in electrophysiological studies. *Psychophysiology*, *49*(4), 549–565. https://doi.org/10.1111/j.1469-8986.2011.01320.x

Maris, E., & Oostenveld, R. (2007). Nonparametric statistical testing of EEG- and MEG-data. *Journal of Neuroscience Methods*, *164*(1), 177–190. https://doi.org/10.1016/j.jneumeth.2007.03.024

Meulman, N., Sprenger, S. A., Schmid, M. S., & Wieling, M. (2023). GAM-based individual difference measures for L2 ERP studies. *Research Methods in Applied Linguistics*, *2*(3), 100079. https://doi.org/10.1016/j.rmal.2023.100079

Meulman, N., Wieling, M., Sprenger, S. A., Stowe, L. A., & Schmid, M. S. (2015). Age Effects in L2 Grammar Processing as Revealed by ERPs and How (Not) to Study Them. *PLOS ONE*, *10*(12), e0143328. https://doi.org/10.1371/journal.pone.0143328

Microsoft, & Weston, S. (2022). *foreach: Provides foreach looping construct*. https://CRAN.R-project.org/package=foreach

Miller, D. L. (2025). Bayesian views of generalized additive modelling. *Methods in Ecology and Evolution*. https://doi.org/10.1111/2041-210x.14498

Mills, B. R. (2022). *MetBrewer: Color palettes inspired by works at the metropolitan museum of art*. https://CRAN.R-project.org/package=MetBrewer

Nalborczyk, L. (2025). *neurogam: Precise temporal localisation of m/EEG effects with bayesian generalised additive multilevel models*. https://github.com/lnalborczyk/neurogam

Nalborczyk, L., Batailler, C., Lœvenbruck, H., Vilain, A., & Bürkner, P.-C. (2019). An Introduction to Bayesian Multilevel Models Using brms: A Case Study of Gender Effects on Vowel Variability in Standard Indonesian. *Journal of Speech, Language, and Hearing Research*, *62*(5), 1225–1242. https://doi.org/10.1044/2018_jslhr-s-18-0006

Nalborczyk, L., Hauw, F., Torcy, H. de, Dehaene, S., & Cohen, L. (in preparation). *Neural and representational dynamics of tickertape synesthesia*.

Pedersen, E. J., Miller, D. L., Simpson, G. L., & Ross, N. (2019). Hierarchical generalized additive models in ecology: An introduction with mgcv. *PeerJ*, *7*, e6876. https://doi.org/10.7717/peerj.6876

Pedersen, T. L. (2024). *patchwork: The composer of plots*. https://CRAN.R-project.org/package=patchwork

Pedersen, T. L., & Crameri, F. (2023). *scico: Colour palettes based on the scientific colour-maps*. https://CRAN.R-project.org/package=scico

Pernet, C. R., Chauveau, N., Gaspar, C., & Rousselet, G. A. (2011). LIMO EEG: A Toolbox for Hierarchical LInear MOdeling of ElectroEncephaloGraphic Data. *Computational Intelligence and Neuroscience*, *2011*, 1–11. https://doi.org/10.1155/2011/831409

Pernet, C. R., Latinus, M., Nichols, T. E., & Rousselet, G. A. (2015). Cluster-based computational methods for mass univariate analyses of event-related brain potentials/fields: A simulation study. *Journal of Neuroscience Methods*, *250*, 85–93. https://doi.org/10.1016/j.jneumeth.2014.08.003

R Core Team. (2025). *R: A language and environment for statistical computing*. R Foundation

for Statistical Computing. https://www.R-project.org/

Rasmussen, C. E., & Williams, C. K. I. (2005). *Gaussian Processes for Machine Learning*. https://doi.org/10.7551/mitpress/3206.001.0001

Rigby, R. A., & Stasinopoulos, D. M. (2005). Generalized Additive Models for Location, Scale and Shape. *Journal of the Royal Statistical Society Series C: Applied Statistics*, *54*(3), 507–554. https://doi.org/10.1111/j.1467-9876.2005.00510.x

Rij, J. van, Hendriks, P., Rijn, H. van, Baayen, R. H., & Wood, S. N. (2019). Analyzing the Time Course of Pupillometric Data. *Trends in Hearing*, *23*. https://doi.org/10.1177/2331216519832483

Riutort-Mayol, G., Bürkner, P.-C., Andersen, M. R., Solin, A., & Vehtari, A. (2023). Practical Hilbert space approximate Bayesian Gaussian processes for probabilistic programming. *Statistics and Computing*, *33*(1), 17. https://doi.org/10.1007/s11222-022-10167-2

Rodriguez-Sanchez, F., & Jackson, C. P. (2024). *grateful: Facilitate citation of R packages*. https://pakillo.github.io/grateful/

Rosenblatt, J. D., Finos, L., Weeda, W. D., Solari, A., & Goeman, J. J. (2018). All-Resolutions Inference for brain imaging. *NeuroImage*, *181*, 786–796. https://doi.org/10.1016/j.neuroimage.2018.07.060

Rousselet, G. A. (2025). Using cluster-based permutation tests to estimate MEG/EEG onsets: How bad is it? *European Journal of Neuroscience*, *61*(1), e16618. https://doi.org/10.1111/ejn.16618

Rousselet, G. A., Pernet, C. R., Bennett, P. J., & Sekuler, A. B. (2008). Parametric study of EEG sensitivity to phase noise during face processing. *BMC Neuroscience*, *9*(1). https://doi.org/10.1186/1471-2202-9-98

Sassenhagen, J., & Draschkow, D. (2019). Cluster-based permutation tests of MEG/EEG data do not establish significance of effect latency or location. *Psychophysiology*, *56*(6). https://doi.org/10.1111/psyp.13335

signal developers. (2023). *signal: Signal processing*. https://r-forge.r-project.org/projects/signal/

Silge, J., & Robinson, D. (2016). tidytext: Text mining and analysis using tidy data principles in r. *JOSS*, *1*(3). https://doi.org/10.21105/joss.00037

Skukies, R., & Ehinger, B. (2021). Modelling event duration and overlap during EEG analysis. *Journal of Vision*, *21*(9), 2037. https://doi.org/10.1167/jov.21.9.2037

Skukies, R., Schepers, J., & Ehinger, B. (2024, December 9). *Brain responses vary in duration - modeling strategies and challenges*. https://doi.org/10.1101/2024.12.05.626938

Slowikowski, K. (2024). *ggrepel: Automatically position non-overlapping text labels with "ggplot2"*. https://CRAN.R-project.org/package=ggrepel

Smith, N. J., & Kutas, M. (2014a). Regression-based estimation of ERP waveforms: I. The rERP framework. *Psychophysiology*, *52*(2), 157–168. https://doi.org/10.1111/psyp.12317

Smith, N. J., & Kutas, M. (2014b). Regression-based estimation of ERP waveforms: II. Nonlinear effects, overlap correction, and practical considerations. *Psychophysiology*, *52*(2), 169–181. https://doi.org/10.1111/psyp.12320

Smith, S., & Nichols, T. (2009). Threshold-free cluster enhancement: Addressing problems of

smoothing, threshold dependence and localisation in cluster inference. *NeuroImage*, *44*(1), 83–98. https://doi.org/10.1016/j.neuroimage.2008.03.061

Sóskuthy, M. (2021). Evaluating generalised additive mixed modelling strategies for dynamic speech analysis. *Journal of Phonetics*, *84*, 101017. https://doi.org/10.1016/j.wocn.2020.101017

Tremblay, A., & Newman, A. J. (2014). Modeling nonlinear relationships in ERP data using mixed-effects regression with R examples. *Psychophysiology*, *52*(1), 124–139. https://doi.org/10.1111/psyp.12299

Umlauf, N., Klein, N., & Zeileis, A. (2018). BAMLSS: Bayesian Additive Models for Location, Scale, and Shape (and Beyond). *Journal of Computational and Graphical Statistics*, *27*(3), 612–627. https://doi.org/10.1080/10618600.2017.1407325

Ushey, K., Allaire, J., & Tang, Y. (2024). *Reticulate: Interface to 'python'*. https://CRAN.R-project.org/package=reticulate

Vaughan, D., & Dancho, M. (2022). *furrr: Apply mapping functions in parallel using futures*. https://CRAN.R-project.org/package=furrr

Vehtari, A., Gelman, A., Simpson, D., Carpenter, B., & Bürkner, P.-C. (2021). Rank-normalization, folding, and localization: An improved R^ for assessing convergence of MCMC (with discussion). *Bayesian Analysis*, *16*(2). https://doi.org/10.1214/20-ba1221

Wickham, H. (2019). *assertthat: Easy pre and post assertions*. https://CRAN.R-project.org/package=assertthat

Wickham, H., Averick, M., Bryan, J., Chang, W., McGowan, L. D., François, R., Grolemund, G., Hayes, A., Henry, L., Hester, J., Kuhn, M., Pedersen, T. L., Miller, E., Bache, S. M., Müller, K., Ooms, J., Robinson, D., Seidel, D. P., Spinu, V., ... Yutani, H. (2019). Welcome to the tidyverse. *Journal of Open Source Software*, *4*(43), 1686. https://doi.org/10.21105/joss.01686

Wickham, H., Pedersen, T. L., & Seidel, D. (2025). *scales: Scale functions for visualization*. https://CRAN.R-project.org/package=scales

Wieling, M. (2018). Analyzing dynamic phonetic data using generalized additive mixed modeling: A tutorial focusing on articulatory differences between L1 and L2 speakers of English. *Journal of Phonetics*, *70*, 86–116. https://doi.org/10.1016/j.wocn.2018.03.002

Wood, S. N. (2003a). Thin Plate Regression Splines. *Journal of the Royal Statistical Society Series B: Statistical Methodology*, *65*(1), 95–114. https://doi.org/10.1111/1467-9868.00374

Wood, S. N. (2003b). Thin-plate regression splines. *Journal of the Royal Statistical Society (B)*, *65*(1), 95–114. https://doi.org/10.1111/1467-9868.00374

Wood, S. N. (2004). Stable and efficient multiple smoothing parameter estimation for generalized additive models. *Journal of the American Statistical Association*, *99*(467), 673–686. https://doi.org/10.1198/016214504000000980

Wood, S. N. (2011). Fast stable restricted maximum likelihood and marginal likelihood estimation of semiparametric generalized linear models. *Journal of the Royal Statistical Society (B)*, *73*(1), 3–36. https://doi.org/10.1111/j.1467-9868.2010.00749.x

Wood, S. N. (2017a). *Generalized Additive Models*. Chapman; Hall/CRC. https://doi.org/10.1201/9781315370279

Wood, S. N. (2017b). *Generalized additive models: An introduction with r* (2nd ed.). Chapman; Hall/CRC.

Wood, S. N. (2017c). *Generalized Additive Models: An introduction with R* (2nd ed.). Chapman; Hall/CRC.

Wood, S. N., Pya, N., & Säfken, B. (2016). Smoothing parameter and model selection for general smooth models (with discussion). *Journal of the American Statistical Association*, *111*, 1548–1575. https://doi.org/10.1080/01621459.2016.1180986

Wüllhorst, V., Wüllhorst, R., Overmeyer, R., & Endrass, T. (2025). Comprehensive Analysis of Event-Related Potentials of Response Inhibition: The Role of Negative Urgency and Compulsivity. *Psychophysiology*, *62*(2). https://doi.org/10.1111/psyp.70000

Xie, Y. (2014). knitr: A comprehensive tool for reproducible research in R. In V. Stodden, F. Leisch, & R. D. Peng (Eds.), *Implementing reproducible computational research*. Chapman; Hall/CRC.

Xie, Y. (2015). *Dynamic documents with R and knitr* (2nd ed.). Chapman; Hall/CRC. https://yihui.org/knitr/

Xie, Y. (2025). *knitr: A general-purpose package for dynamic report generation in R*. https://yihui.org/knitr/

Xie, Y., Allaire, J. J., & Grolemund, G. (2018). *R markdown: The definitive guide*. Chapman; Hall/CRC. https://bookdown.org/yihui/rmarkdown

Xie, Y., Dervieux, C., & Riederer, E. (2020). *R markdown cookbook*. Chapman; Hall/CRC. https://bookdown.org/yihui/rmarkdown-cookbook

Yeung, N., Bogacz, R., Holroyd, C. B., & Cohen, J. D. (2004). Detection of synchronized oscillations in the electroencephalogram: An evaluation of methods. *Psychophysiology*, *41*(6), 822–832. https://doi.org/10.1111/j.1469-8986.2004.00239.x

Appendix A
Application to 2D time-resolved decoding results (cross-temporal generalisation)

We conducted a cross-temporal generalisation analysis of the decoding data from Nalborczyk et al. (in preparation), in which we assessed the performance of classifiers trained and tested at various timesteps of the trial (King & Dehaene, 2014). This analysis was performed at the participant level, resulting in a 2D matrix where each element contains the decoding accuracy (ROC AUC) of a classifier trained at timestep training$_i$ and tested at timestep testing$_j$ for each participant (Figure A1).

Figure A1

Group-level average cross-temporal generalisation matrix of decoding performance (data from Nalborczyk et al., in preparation).

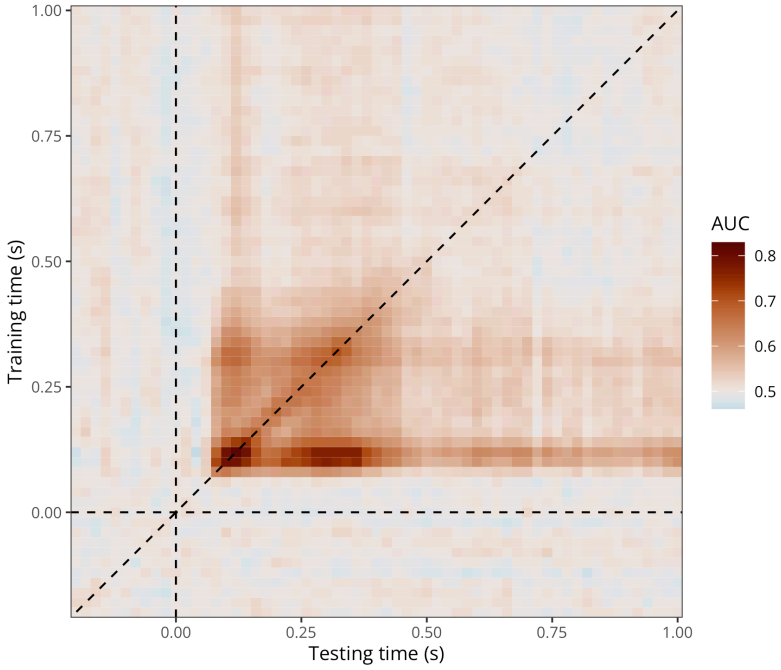

To model cross-temporal generalisation matrices of decoding performance, we extended our initial BGAM to take into account the bivariate temporal distribution of AUC values, thus producing naturally smoothed estimates (timecourses) of AUC values and posterior odds. This model can be written as follows:

$$\begin{aligned} \text{AUC}_i &\sim \text{Beta}\left(\mu_i, \phi\right) \\ \text{logit}\left(\mu_i\right) &= \alpha + f\left(\text{train}_i, \text{test}_i\right) \\ f\left(\text{train}_i, \text{test}_i\right) &\equiv \sum_{k=1}^{K} b_k B_k\left(\text{train}_i, \text{test}_i\right) \end{aligned}$$

where AUC values are assumed to follow a Beta distribution, parametrised by a mean μ_i and a precision parameter ϕ. The mean μ_i is linked to the predictors through a logit link function. The smooth function $f(\text{train}_i, \text{test}_i)$ represents a two-dimensional surface defined over training and testing times, which captures how decoding performance varies across the temporal gen-

eralisation matrix. This surface is approximated by a linear combination of K basis functions $B_k(\cdot, \cdot)$, each weighted by a coefficient b_k. The basis functions are constructed using a tensor product of univariate splines (here thin-plate splines) applied to the training and testing time dimensions (Wood, 2003a, 2017a).

We fitted this model using `brms` and the `t2()` tensor product smooth constructor with full penalties (E. J. Pedersen et al., 2019; Wood, 2017a). We ran eight MCMCs to approximate the posterior distribution, including each 5000 iterations and a warmup of 1000 iterations, yielding a total of $8 \times (5000 - 1000) = 32000$ posterior samples to be used for inference.

```
# fitting a GAM with two temporal dimensions
timegen_gam <- brm(
    # 2D thin-plate spline (tp) with full penalties
    auc ~ t2(train_time, test_time, bs = "tp", k = 30, full = TRUE),
    data = timegen_data,
    family = Beta(),
    warmup = 1000,
    iter = 5000,
    chains = 8,
    cores = 8,
    control = list(adapt_delta = 0.95, max_treedepth = 15)
    )
```

Figure A2

Predicted AUC values with threshold (left) and posterior odds of decoding accuracy being above chance (right) according to the bivariate BGAM.

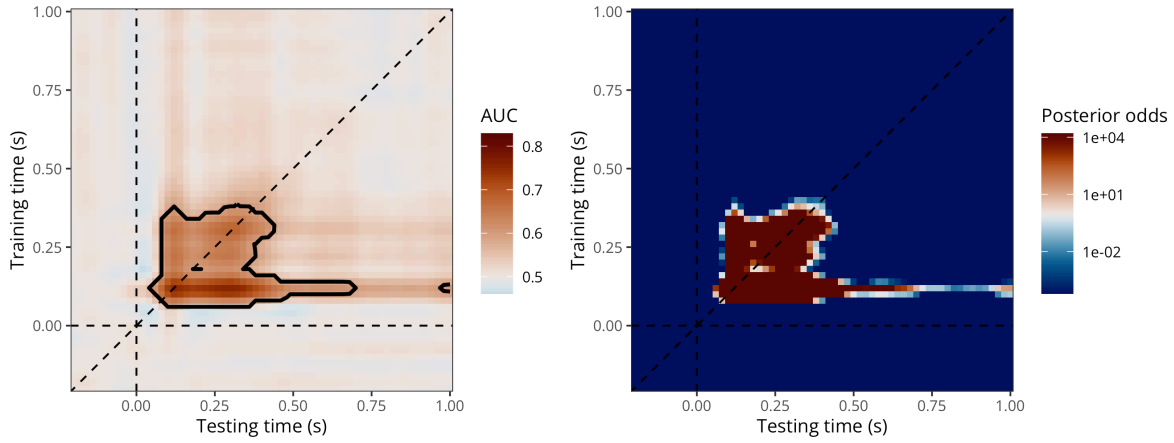

Figure A2 shows the predictions from the model (left) superimposed with the identified cluster as defined by thresholding the posterior odds (right). Notably, this model could be extended to a multilevel bivariate GAM via `t2(train_time, test_time, participant, bs = c("tp",`

658 `"tp", "re"), m = 2, full = TRUE)` and could be generalised to account for both spatial (`x`
659 and `y`) and temporal (`time`) dimensions with formulas such as `te(x, y, time, d = c(2, 1)`
660 `)`.

Table B1

Models comparison with LOOIC. Models are arranged by the diffence in expected log-pointwise density (ELPD) to the best model (i.e., k=40).

k	elpd_diff	se_diff	elpd_loo	se_elpd_loo	p_loo	se_p_loo	looic	se_looic
40	0.00	0.00	5,579.11	69.47	47.79	0.74	-11,158.21	138.94
80	-0.63	0.38	5,578.47	69.48	50.30	0.78	-11,156.94	138.97
20	-6.43	3.38	5,572.68	69.59	36.99	0.58	-11,145.35	139.17
10	-36.12	8.85	5,542.98	69.88	19.29	0.32	-11,085.97	139.76
5	-1,605.12	53.40	3,973.99	71.54	11.13	0.19	-7,947.98	143.09

Appendix B
How to choose the GAM basis dimension?

There is no universal recommendation for choosing the optimal value of `k`, as it depends on several factors, including the sampling rate, preprocessing steps (e.g., signal-to-noise ratio, low-pass filtering), and the underlying neural dynamics of the phenomenon under investigation. One strategy is to set `k` as high as computational constraints allow, as suggested by previous authors (e.g., E. J. Pedersen et al., 2019). Alternatively, one can fit a series of models with different `k` values and compare them using information criteria such as LOOIC or WAIC, alongside posterior predictive checks (PPCs), to select the model that best captures the structure of the data. We illustrate this approach below.

Figure B1 presents the posterior predictions and two forms of posterior predictive checks (PPCs) for each GAM fit using different numbers of basis functions ($k \in \{5, 10, 20, 40, 80\}$). With the exception of the $k = 5$ model, all other fits yield satisfactory PPCs, indicating that the predicted data closely resemble the empirical observations. However, model comparison using the leave-one-out information crtierio (LOOIC), as summarised in Table 1, identifies the $k = 40$ model as the best-performing one in terms of LOOIC, closely followed by the $k = 80$ model. This suggests that the optimal number of basis functions likely lies between these two values. Future simulation studies could further investigate how such model selection criteria relate to the precision of onset and offset estimates.

Figure B1

Posterior predictions and posterior predictive checks for the GAM with varying k (in rows).

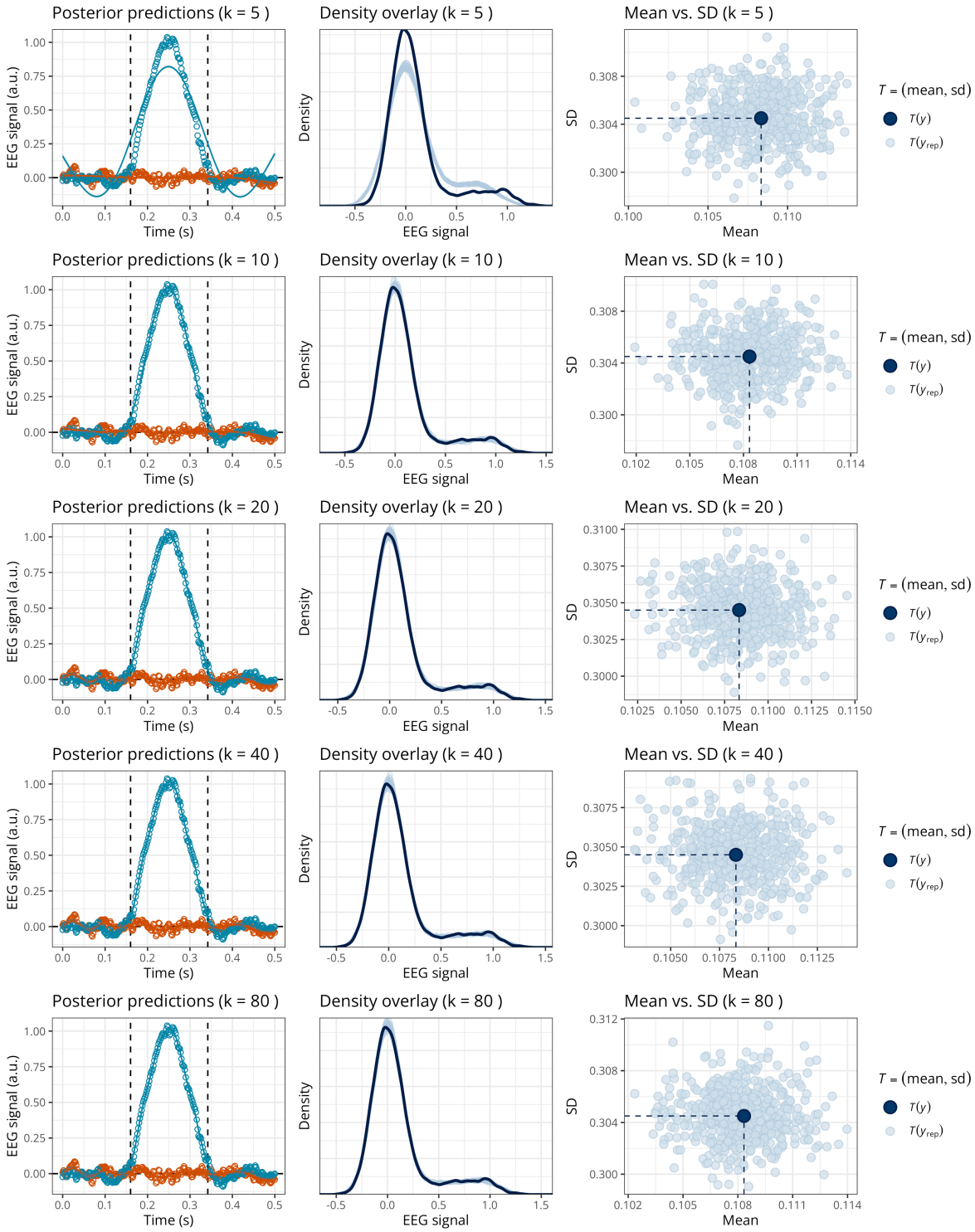

Appendix C
`R` package and integration with `MNE-Python`

For readers who are already familiar with `brms`, the recommended pipeline is to use the code provided in the main paper (available at https://github.com/lnalborczyk/brms_meeg). It is also possible to call functions from the `neurogam R` package (available at https://github.com/lnalborczyk/neurogam) which come with sensible defaults.

```r
# installing (if needed) and loading the neurogam R package
# remotes::install_github("https://github.com/lnalborczyk/neurogam")
library(neurogam)

# using the testing_through_time() function from the neurogam package
# this may take a few minutes (or hours depending on the machine's
# performance and the size of the dataset)...
gam_onset_offset <- testing_through_time(
    # dataframe with M/EEG data in long format
    data = raw_df,
    # the *_id arguments are used to specify the relevant columns in data
    participant_id = "participant", meeg_id = "eeg",
    time_id = "time", predictor_id = "condition",
    # posterior odds threshold for defining clusters (20 by default)
    threshold = 20,
    # number of warmup MCMC iterations
    warmup = 1000,
    # total number of MCMC iterations
    iter = 5000,
    # number of MCMCs
    chains = 4,
    # number of parallel cores to use for running the MCMCs
    cores = 4
    )

# displaying the results
gam_onset_offset$clusters
```

The `neurogam` package can also be called from `Python` using the `rpy2` module, and can easily be integrated into `MNE-Python` pipelines. For example, we use it below to estimate the onset and offset of effects for one EEG channel from an MNE evoked object. The code used to reshape the `sample MNE` dataset is available in the online supplementary materials, and we further refer to the MNE documentation about converting `MNE` epochs to `Pandas` dataframes in long format (i.e., with one observation per row).

```
# loading the Python modules
import rpy2.robjects as robjects
from rpy2.robjects.packages import importr
from rpy2.robjects import pandas2ri
from rpy2.robjects.conversion import localconverter

# importing the "neurogam" R package
neurogam = importr("neurogam")

# activating automatic pandas-R conversion
pandas2ri.activate()

# assuming reshaped_df is some M/EEG data reshaped in long format
with localconverter(robjects.default_converter + pandas2ri.converter):

    reshaped_df_r = robjects.conversion.py2rpy(reshaped_df)


# using the testing_through_time() function from the neurogam R package
gam_onset_offset = neurogam.testing_through_time(
    data=reshaped_df_r,
    threshold=20,
    multilevel=False
    )

# displaying the results
print(list(gam_onset_offset) )
```